Supporting Information

Tan et al. 10.1073/pnas.1717815115

SI Materials and Methods

Animals. The following mouse lines were used: Atoh1-CreER (1), $En1^{CreER}$ (2), Atoh1-FlpoER and $Rosa26^{MASTR(frt\text{-}STOP\text{-}frt\text{-}GFPcre)}$ (3) and $R26^{LSL\text{-}SmoM2\text{-}YFP}$ (4), $Ptch1^{flox/flox}$ (5), $Nr2f2^{flox/flox}$ (6), $En1^{flox/flox}$ (7), $En2^{flox/flox}$ (8), and Atoh1-GFP (9). All mouse lines besides $R26^{LSL\text{-}SmoM2\text{-}YFP}$ and $Nr2f2^{flox/flox}$ (C57BL/6 inbred) were maintained on an outbred Swiss Webster background and both sexes were used for the analysis. Animals were housed on a 12-h light/dark cycle and were given access to food and water ad libitum. All experiments were performed using mice from embryonic stages to adult (ages E14.5–P300).

To induce genetic recombination, Tm (Sigma-Aldrich) was dissolved in corn oil (Sigma-Aldrich) at 20 mg/mL. Before each injection, Tm was freshly diluted and given in one dose to P2 *Atoh1-CreER/+;*$R26^{LSL\text{-}SmoM2\text{-}YFP}$ (*A-SmoM2*) mice at 0.5–1 μg/g via subcutaneous injection. For $En1^{CreER/+}$;$R26^{LSL\text{-}SmoM2\text{-}YFP/+}$, *Atoh1-FlpoER/+;*$Rosa26^{MASTR/SmoM2\text{-}YFP}$ (*A-M-SmoM2*), *Atoh1-FlpoER/+;*$Rosa26^{MASTR/SmoM2\text{-}YFP}$;$Ptch1^{flox/flox}$ (*A-M-Ptch*), *Atoh1-FlpoER/+;*$Rosa26^{MASTR/SmoM2\text{-}YFP}$;$Nr2f2^{flox/flox}$(*A-M-SmoM2-N*), *Atoh1-FlpoER/+;*$Rosa26^{MASTR/SmoM2\text{-}YFP}$;$Nr2f2^{flox/+}$(*A-M-SmoM2-N* het), and *Atoh1-FlpoER/+;*$Rosa26^{MASTR/SmoM2\text{-}YFP}$;$En1^{flox/flox}$; $En2^{flox/flox}$ (*A-M-SmoM2-E*), mice were given one dose of 200 μg/g Tm at P2 via subcutaneous injection. To induce genetic recombination of *Atoh1-CreER/+;*$R26^{LSL\text{-}SmoM2\text{-}YFP}$ mice at an embryonic stage (E14.5), 5 μg/g Tm was given to the mother intraperitoneally.

Histology and IHC. For histological analysis, animals were perfused with cold PBS followed by 4% paraformaldehyde (PFA). Whole brains were extracted and fixed in 4% PFA overnight (early postnatal brains) or for 2 d (brains with tumor) at 4 °C. Tissues were then transferred to 30% sucrose for 24–48 h, processed for frozen embedding in optimal cutting temperature (OCT) compound, and sectioned in sagittal plane on a Leica cryostat at 14 μm. For IHC, sections were blocked for at least 1 h in 5% BSA (Sigma-Aldrich) and 0.3% Triton X-100 (Fisher Scientific) and incubated overnight at 4 °C with the following primary antibodies: rat anti-GFP (04404-84; Nacalai Tesque), rabbit anti-K_i67 (RM-9106-S0; Thermo Scientific), rabbit anti-EN1/2 (10), and rabbit anti-NR2F2 (6434; Cell Signaling). P27 immunostaining (mouse anti-P27, 610241; BD Pharmingen) required 40-min antigen retrieval (pH 6, 10 mM Sodium Citrate, 0.05% Tween) at 95 °C before blocking. Sections were then incubated for 1 h at room temperature (20–25 °C) with secondary species-specific antibodies conjugated with the appropriate Alexa Fluor (1:1,000: Alexa Fluor-555 donkey anti-rabbit, A-31572; Alexa Fluor-488 donkey anti-rat IgG, A21208; Alexa Fluor-488 donkey anti-mouse, A21202; Invitrogen). For GFP staining of P4 *A-SmoM2* brains, sections were incubated with 0.03% H_2O_2 for 10 min, blocked for 1 h, incubated with rat anti-GFP antibody overnight, and then with biotin donkey anti-rat secondary antibody (712-065-153; Jackson Immuno Research) for 1 h at room temperature. ABC kit (Vectastain) followed by 30-min incubation with 3,3′-Diaminobenzidine (Sigma-Aldrich) was used to detect GFP^+ cells. EdU was detected using a commercial kit (C10340; Invitrogen). Images were collected on a DM6000 Leica microscope, Zeiss inverted microscope (Observer.Z1), or Nanozoomer S210 slide scanner (Hamamatsu) and processed using Photoshop software.

RNA in Situ Hybridization. The in situ hybridization was performed as previously described (11, 12) using *En1* (13), *Nr2f2*, and *EphA3* antisense RNA probes. The template for *Nr2f2* and *EphA3* probes were generated by PCR using primers containing T7 or SP6 polymerase promoters from postnatal cerebellum cDNA. The following primer pairs were used: *Nr2f2*: F 5′ GCCACTCGTACCTGTCCGGA3′ and R 5′ GCTTTCCACATGGGCTACAT3′; *EphA3*: F 5′ TCGATATCGCTACCTTCCACACAA3′ and R 5′ ACTTGCCCCCAAATTAAGACGTG3′.

Mosaic Analysis of GCPs Undifferentiated State and Proliferation Index. Mice were injected with 200 μg/g Tm at P2 and killed at P8 for analysis. Fifty micrograms of EdU (Invitrogen) per gram of body weight was administered via intraperitoneal injection (10 mg/mL in sterile saline) 1 h before being killed. For undifferentiated state analysis, the number of nuclear GFP^+ (MASTR allele) cells in the proliferating outer EGL (marked by K_i67) and the total number of GFP^+ cells were counted from three sections per location. For each mouse, the percentage of undifferentiated GCPs in each location was calculated as the percent of GFP^+ cells in the proliferating outer EGL/total GFP^+ cells. For proliferation index, the number of GFP^+ EdU^+ cells in the proliferating outer EGL (K_i67^+) and the total number of GFP^+ cells in the outer EGL were counted from three sections per location. Proliferation index was calculated as the percent GFP^+ EdU^+ cells/GFP^+ cells in outer EGL.

MEMRI. Mice were given an intraperitoneal injection of 30 mM $MnCl_2$ in isotonic saline (62.5 mg per kilogram of body weight) 24 h before imaging. MRI data were acquired on a 7-Tesla microimaging scanner (Bruker Biospin) using a 3D gradient echo sequence (echo/repetition time, TE/TR = 4/30-ms; flip angle = 20°; matrix size = 128 × 128 × 64) yielding 150-μm isotropic resolution in ∼20 min. Three-dimensional MEMRI images were analyzed using Amira (v5.5.0; Visage Imaging), generating segmented tumor volumes, as described previously (14).

Cell Isolation and Orthotopic Transplantation. For P8: cerebella of *Atoh1-CreER/+;*$R26^{LSL\text{-}SmoM2\text{-}YFP}$ mice (200 μg/g Tm at P2) were dissected out and separated into H or V regions under the dissection microscope. Tissues were digested by Trypsin/DNase and the mutant GCPs were enriched by a Percoll gradient method (15). For P21: cerebella of *Atoh1-CreER/+;*$R26^{LSL\text{-}SmoM2\text{-}YFP}$ mice (5 μg/g Tm at P2) were dissected out and processed as for P8 samples. A volume of 3 μL containing 5×10^5 mutant cells from the H or V was injected into the right hemisphere of athymic nude mice ($Foxn1^{nu/nu}$) by using a Hamilton syringe and automated stereotaxic equipment (Kopf Instruments, model 900).

qRT-PCR. RNA was isolated from FACS-isolated GFP^+ cells from P8 *Atoh1-GFP* mice and FACS-isolated YFP^+ cells from *Atoh1-SmoM2* tumor using a miRNeasy Micro Kit (Qiagen) according to the manufacturer's protocol. cDNA was prepared using iScript cDNA synthesis kit (Bio-Rad). qRT-PCR was performed using PowerUp Sybr Green Master Mix (Applied Biosystems). Fold-changes in expression were calculated using the ΔΔCt method. The *Gapdh* gene was used to normalize the results. The following primer pairs were used: *Nr2f2*: F 5′ TCAACTGCCACTCGTACCTG3′ and R 5′CCATGATGTTGTTAGGCTGCAT3′; *EphA3*: F 5′ TTCTCCATCTCCGGTGAAAACA3′ and R 5′ ACCTCCCGACCAGAACATAGG3′; *En1*: F 5′ CTAAGGCCCGATTTCGGTTG3′ and R 5′ GAGTGAACGGGGTCTCTACCT3′; *Gapdh*: F 5′ CCAAGGTGTCCGTCGTGGATCT3′ and R 5′ GTTGAAGTCGCAGGAGACAACC3′.

Microarray Analysis. P8 WT GCPs or *SmoM2*-mutant GCPs (*Atoh1-CreER/+;*$R26^{LSL\text{-}SmoM2\text{-}YFP}$; 200 ug/g Tm at P2) were isolated by Percoll gradient. The Memorial Sloan Kettering Cancer

Center Integrated Genomics Operation core facility performed RNA isolation and microarray analysis. Briefly, high-quality RNA were interrogated with Affymetrix microarrays (GeneChip Mouse Genome 430 2.0 Array). GeneChip CEL files were analyzed with the Partek Genomics Suite and Gene Pattern, including unsupervised hierarchical clustering strategies and PCA. Supervised analyses comprised LIMMA, ANOVA, and SAM to infer specific gene sets.

Quantifications and Statistical Analyses. Quantification of lesion size (in square millimeters) at P45 and symptomatic was using ImageJ software. Preneoplastic lesions were defined as <0.5 mm^2 and tumors as >0.5 mm^2. The area of lesions in the H and V of each mouse were measured from the sagittal section, with the total lesion/tumor in each location. Comparing the H lesion size between *A-M-SmoM2*, *A-M-SmoM2-N*, and *A-M-SmoM2-N* het was done by quantifying the area (in square millimeters) of the largest lesion per sagittal section per mouse. Mice used for this comparison were generated from three separate crosses that produced *A-M-SmoM2* alone, *A-M-SmoM2*, and *A-M-SmoM2-N* het littermates, and *A-M-SmoM2-N* het and *A-M-SmoM2-N* littermates. Quantification of the differentiation state (percent of $P27^+$ over $DAPI^+$ area) of P21 preneoplastic lesions was also done using ImageJ software. The lesions were identified by GFP^+ staining and the area of $P27^+$ cells were quantified on the adjacent section. Three lesions per location per mouse were quantified. All statistical analyses were performed using Prism software (GraphPad) and significance was determined as $P < 0.05$. Survival curve comparisons were determined by a log-rank (Mantel-Cox) test. All other statistical analyses were two-tailed unless specified. A paired Student's *t* test was used for comparison between the H and V within mice of one model. One-way ANOVA with Tukey post hoc test was used for multiple genotype comparisons. Two-way ANOVA with a Sidak post hoc test was used for comparing differences between locations and different genotypes. *P* values and degrees of freedom are given in the Table S2. No statistical methods were used to predetermine the sample size, but our sample sizes are similar to those generally employed in the field. No randomization was used. Data collection and analysis were not performed blind to the conditions of the experiments, in part because genotype was often obvious.

1. Machold R, Fishell G (2005) Math1 is expressed in temporally discrete pools of cerebellar rhombic-lip neural progenitors. *Neuron* 48:17–24.
2. Sgaier SK, et al. (2005) Morphogenetic and cellular movements that shape the mouse cerebellum; insights from genetic fate mapping. *Neuron* 45:27–40.
3. Lao Z, Raju GP, Bai CB, Joyner AL (2012) MASTR: A technique for mosaic mutant analysis with spatial and temporal control of recombination using conditional floxed alleles in mice. *Cell Reports* 2:386–396.
4. Mao J, et al. (2006) A novel somatic mouse model to survey tumorigenic potential applied to the Hedgehog pathway. *Cancer Res* 66:10171–10178.
5. Ellis T, et al. (2003) Patched 1 conditional null allele in mice. *Genesis* 36:158–161.
6. Takamoto N, et al. (2005) COUP-TFII is essential for radial and anteroposterior patterning of the stomach. *Development* 132:2179–2189.
7. Sgaier SK, et al. (2007) Genetic subdivision of the tectum and cerebellum into functionally related regions based on differential sensitivity to engrailed proteins. *Development* 134:2325–2335.
8. Cheng Y, et al. (2010) The engrailed homeobox genes determine the different foliation patterns in the vermis and hemispheres of the mammalian cerebellum. *Development* 137:519–529.
9. Chen P, Johnson JE, Zoghbi HY, Segil N (2002) The role of Math1 in inner ear development: Uncoupling the establishment of the sensory primordium from hair cell fate determination. *Development* 129:2495–2505.
10. Davis CA, Holmyard DP, Millen KJ, Joyner AL (1991) Examining pattern formation in mouse, chicken and frog embryos with an En-specific antiserum. *Development* 111:287–298.
11. Blaess S, et al. (2011) Temporal-spatial changes in Sonic Hedgehog expression and signaling reveal different potentials of ventral mesencephalic progenitors to populate distinct ventral midbrain nuclei. *Neural Dev* 6:29.
12. Wassarman KM, et al. (1997) Specification of the anterior hindbrain and establishment of a normal mid/hindbrain organizer is dependent on Gbx2 gene function. *Development* 124:2923–2934.
13. Millen KJ, Hui CC, Joyner AL (1995) A role for En-2 and other murine homologues of *Drosophila* segment polarity genes in regulating positional information in the developing cerebellum. *Development* 121:3935–3945.
14. Suero-Abreu GA, et al. (2014) In vivo Mn-enhanced MRI for early tumor detection and growth rate analysis in a mouse medulloblastoma model. *Neoplasia* 16:993–1006.
15. Gao WO, Heintz N, Hatten ME (1991) Cerebellar granule cell neurogenesis is regulated by cell-cell interactions in vitro. *Neuron* 6:705–715.

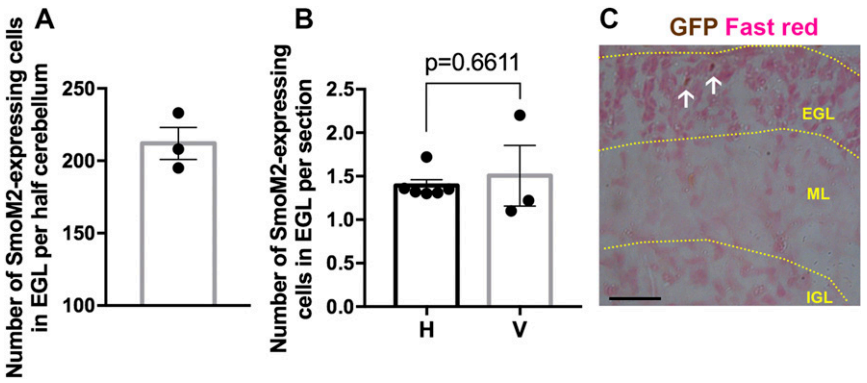

Fig. S1. No preferential recombination between the H and V in *A-SmoM2* mice given 1 μg/g Tm. (*A*) Quantification of SmoM2-expressing cells located in the EGL of P4 *A-SmoM2* mice given 1 μg/g Tm at P2 (mean: 212 ± 11.15 cells; $n = 3$). The entire P4 cerebella were sectioned (14 μm), and every other section was stained to detect YFP and quantified (~146 sections). (*B*) The number of SmoM2-expressing cells located in the EGL per section for the V (45–51 sections) and one hemisphere/paravermis (42–61 sections) [H: 1.39 ± 0.07 YFP^+ cells per section, $n = 6$ (3 left and 3 right); V: 1.51 ± 0.35 YFP^+ cells per section, $n = 3$]. Significance was determined using unpaired Student's *t* test. All data are expressed as mean ± SEM. (*C*) Representative image of IHC staining showing cells labeled with a GFP antibody (white arrows) located in the EGL of a P4 *A-SmoM2* mouse. EGL, ML, and IGL are indicated with yellow dotted lines. (Scale bar, 25 μm.)

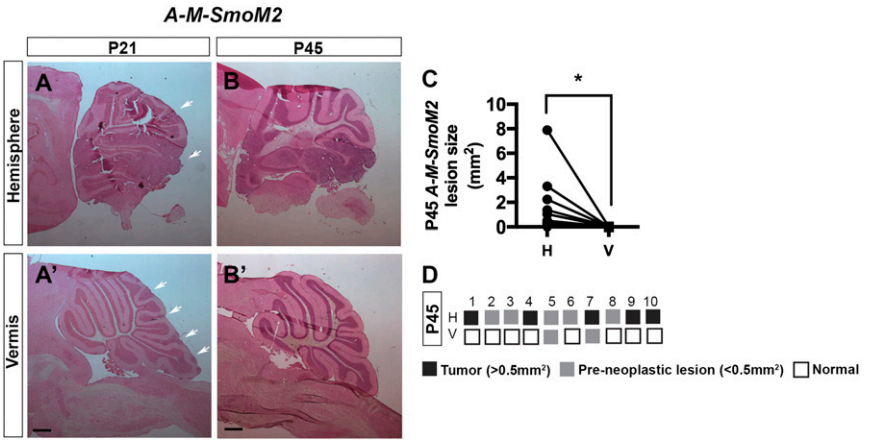

Fig. S2. *A-M-SmoM2* mice have similar tumor progression profiles to *A-SmoM2* (Fig. 1). (*A* and *B*) H&E staining of sagittal sections in the H and V (*A′* and *B′*) of the cerebellum of *A-M-SmoM2* mice (*Atoh1-FlpoER/+;R26*$^{MASTR/LSL\text{-}SmoM2}$ mice given a high dose of Tm at P2) at P21 (*A*) and P45 (*B*). White arrows indicate lesions that had nuclear GFP staining. Some lesions in this model, and not in the *A-M-Ptch* model, do not express nuclear GFP due to transient "leaky" expression of eGFPcre at a random stage of development (3). (Scale bars, 500 μm.) (*C*) Graphs representing the size of nuclear GFP$^+$ lesions in the H and V of P45 *A-M-SmoM2* mice [H: 1.73 ± 0.759 mm^2; V: 0.0071 ± 0.0048 mm^2; $n = 10$; $P = 0.0496$, $t(9) = 2.267$]. Significance was determined using paired Student's *t* test, $^*P < 0.05$. (*D*) Schematic representation showing the presence of nuclear GFP$^+$ tumors or preneoplastic lesions in individual P45 *A-M-SmoM2* mice.

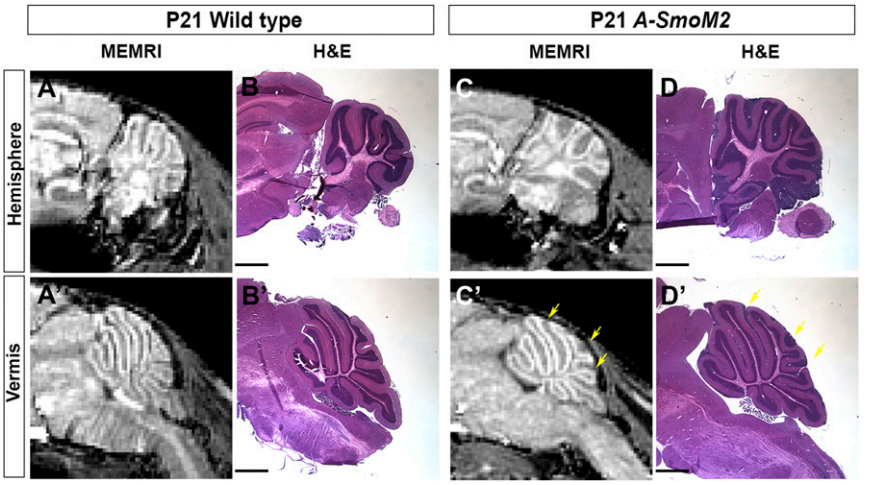

Fig. S3. MEMRI allows detection of preneoplastic lesions as early as P21. (*A* and *C*) Sagittal MEMRI images in the H and V (*A′* and *B′*) of P21 WT (*A*) and *A-SmoM2* (*C*) mice. (*B* and *D*) Matched H&E staining of sagittal sections in H and V (*B′* and *D′*) of the same WT (*B*) and *A-SmoM2* (*D*) cerebellum at P21. Yellow arrows indicate lesions. (Scale bars, 500 μm.)

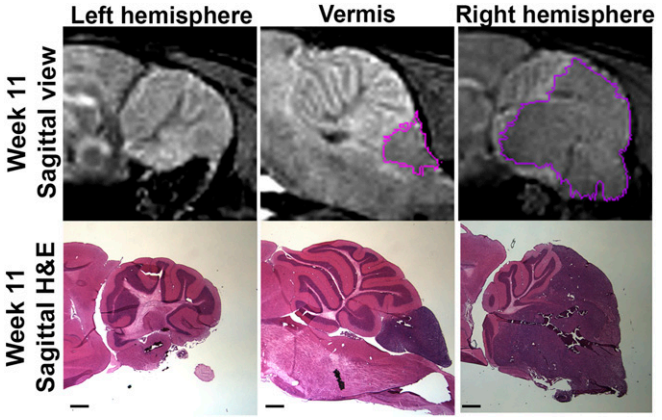

Fig. S4. MEMRI confirms an advanced *A-SmoM2* tumor grew from one hemisphere to the medial cerebellum. MEMRI sagittal views and matched H&E-stained sections in left and right H and V of 11-wk *A-SmoM2* mouse shown in Fig. 2. Lesions/tumors are outlined by purple lines. (Scale bars, 500 μm.)

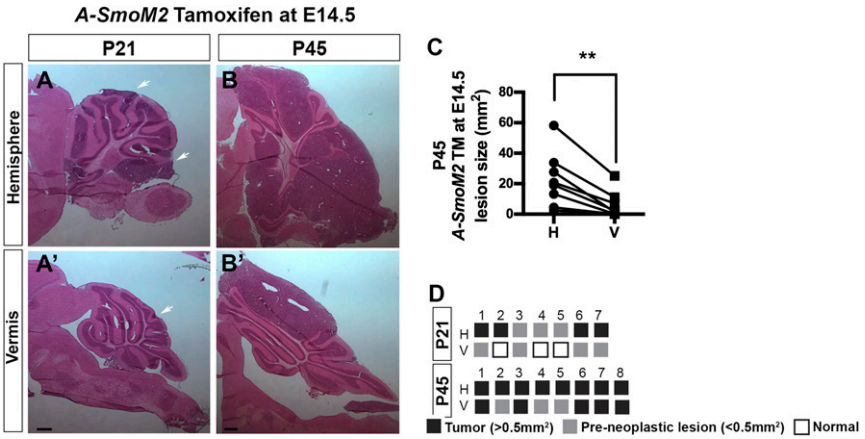

Fig. S5. Tumors are preferentially located in the H of *A-SmoM2* administered Tm at E14.5. (*A* and *B*) H&E staining of sagittal sections in the H and V (*A′* and *B′*) of P21 (*A*) and P45 (*B*) *A-SmoM2* mice administered Tm at E14.5. White arrows indicate lesions. (Scale bars, 500 μm.) (*C*) Graphs representing the size of lesions in the H and V of P45 *A-M-SmoM2* mice [H: 22.46 ± 6.34 mm^2; V: 5.98 ± 3.07 mm^2; $n = 8$; $P = 0.0030$, $t(7) = 4.436$]. Significance was determined using paired Student's *t* test, $^{**}P < 0.01$. (*D*) Schematic representation showing the presence of tumors or preneoplastic lesions in individual P21 and P45 *A-SmoM2* mice administered Tm at E14.5.

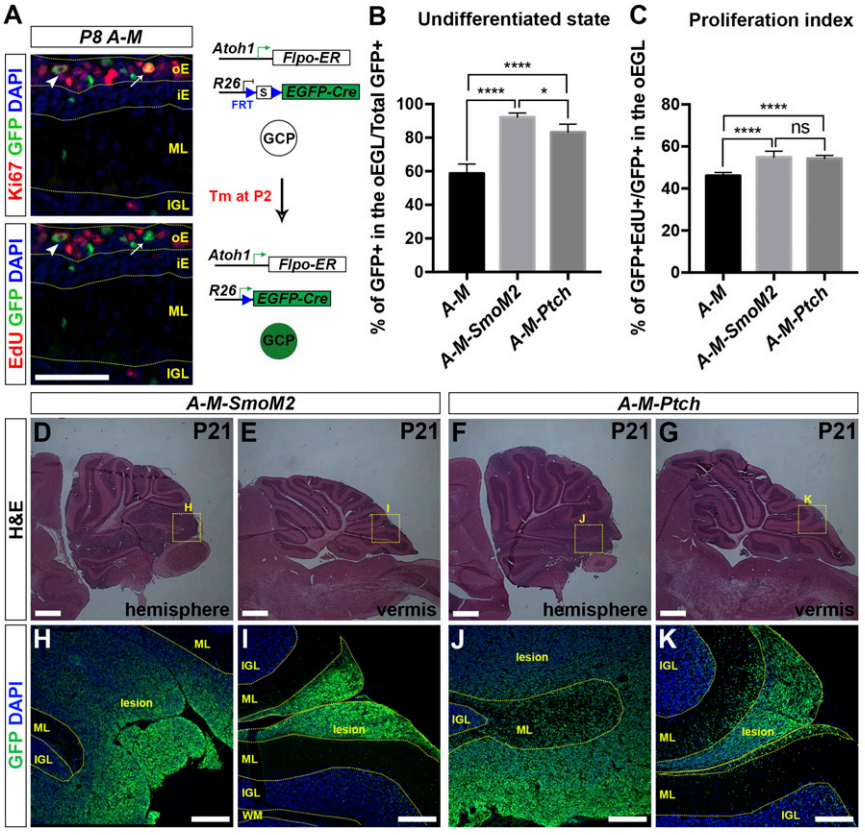

Fig. S6. Elevated SHH signaling in GCPs keeps cells in an undifferentiated state and increases the proliferation index. (*A*) FIHC detection of the indicated proteins and DAPI on a representative section of P8 *A-M* mouse to illustrate the method of quantifying undifferentiated cells (percent GFP^+ cells in the proliferating outer EGL/total GFP^+ cells) and proliferation index (percent GFP^+ EdU^+ cells/GFP^+ cells in the outer EGL). The EGL was separated into an inner EGL (iE; K_i67^-) outer EGL (oE; K_i67^+). The IGL and ML are indicated and outlined by yellow dotted lines. White arrows indicate GFP^+K_i67 cells and arrowheads indicate $GFP^+K_i67^+EdU^+$ cells in the oE. Next to the images is a schematic representation of the MASTR approach. (Scale bar, 50 μm.) (*B*) Graphs of the percentage of undifferentiated GCPs of P8 *A-M* ($n = 4$), *A-M-SmoM2* ($n = 3$), and *A-M-Ptch* ($n = 3$) mice [one-way ANOVA, $F_{(2, 17)} = 98.97$, $P < 0.0001$]. (*C*) Graphs of the proliferation index comparing P8 *A-M* ($n = 4$), *A-M-SmoM2* ($n = 3$), and *A-M-Ptch* ($n = 3$) mice [one-way ANOVA, $F_{(2, 17)} = 40.96$, $P < 0.0001$]. *P* values of Tukey post hoc pairwise comparison are shown in the figure. All data are expressed as mean ± SEM; $^*P < 0.05$, $^{****}P < 0.0001$. (*D–G*) H&E staining of sagittal sections in the H (*D* and *F*) and V (*E* and *G*) of P21 *A-M-SmoM2* (*D* and *E*) and *A-M-Ptch* (*F* and *G*) mice administrated Tm at P2. (Scale bars, 1 mm.) (*H–K*) FIHC detection of GFP and DAPI on sagittal sections of P21 *A-M-SmoM2* and *A-M-Ptch* mice in the regions outlined by the dotted squares in *D–G*. IGL, ML, and lesions are indicated with yellow dotted lines. (Scale bars, 200 μm.)

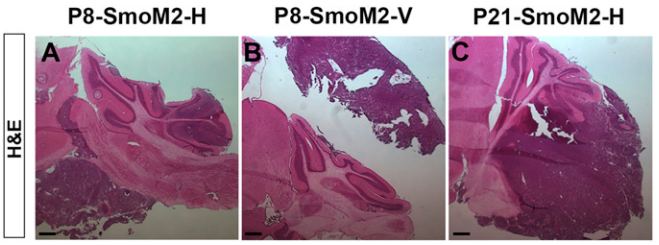

Fig. S7. Histology of transplanted tumors resembles *A-SmoM2* tumors. H&E staining of sagittal right H sections from symptomatic P8-SmoM2-H (*A*), P8-SmoM2-V (*B*), and P21-SmoM2-H (*C*) mice. (Scale bars, 500 μm.)

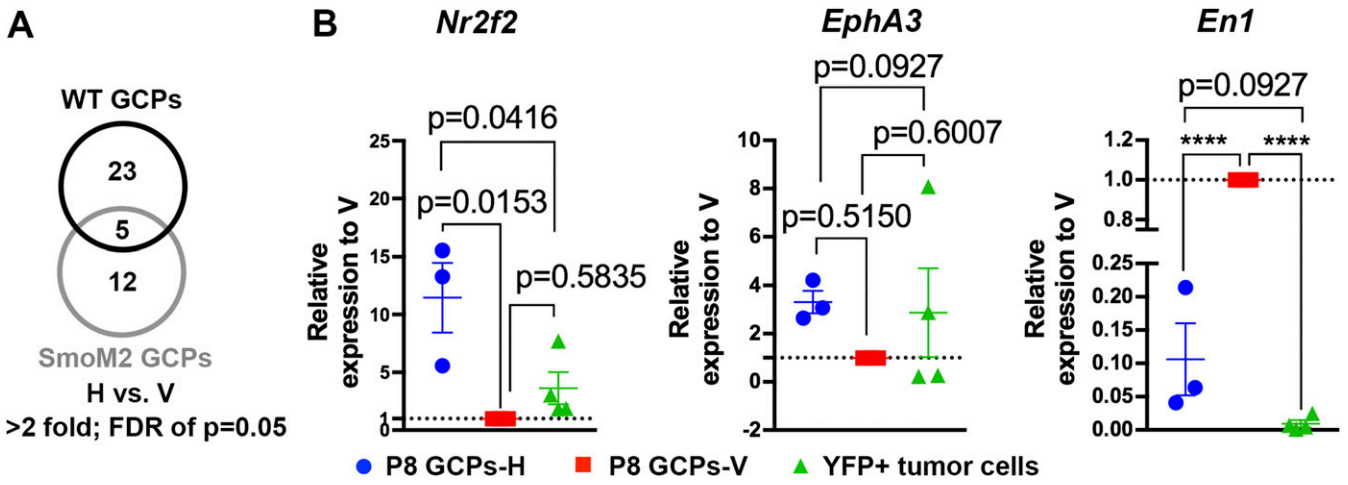

Fig. S8. Microarray analysis identifies different gene expression profiles between GCPs isolated from the H and V. (*A*) Venn diagram showing number of genes differentially expressed between H and V GCPs isolated from P8 WT and *A-SmoM2* mice (high-dose Tm). (*B*) qRT-PCR analysis of the indicated genes in GFP^+ GCPs sorted from the H (P8 GCPs-H, $n = 3$ FACS experiments) or V (P8 GCPs-V, $n = 3$ FACS experiments) of WT P8 *Atoh1-GFP/+* cerebella and of sorted YFP^+ tumor cells from *A-SmoM2* mice ($n = 4$ FACS experiments). One-way ANOVA overall *P* value for *Nr2f2* $F_{(2,\ 7)} = 8.128$, $P = 0.0150$, *EphA3* $F_{(2,\ 7)} = 0.7671$, $P = 0.4998$, and *En1* $F_{(2,\ 7)} = 370.5$, $P < 0.0001$. *P* values of Tukey post hoc pairwise comparison are shown in the figure, $^{****}P < 0.0001$. All data are expressed as mean ± SEM.

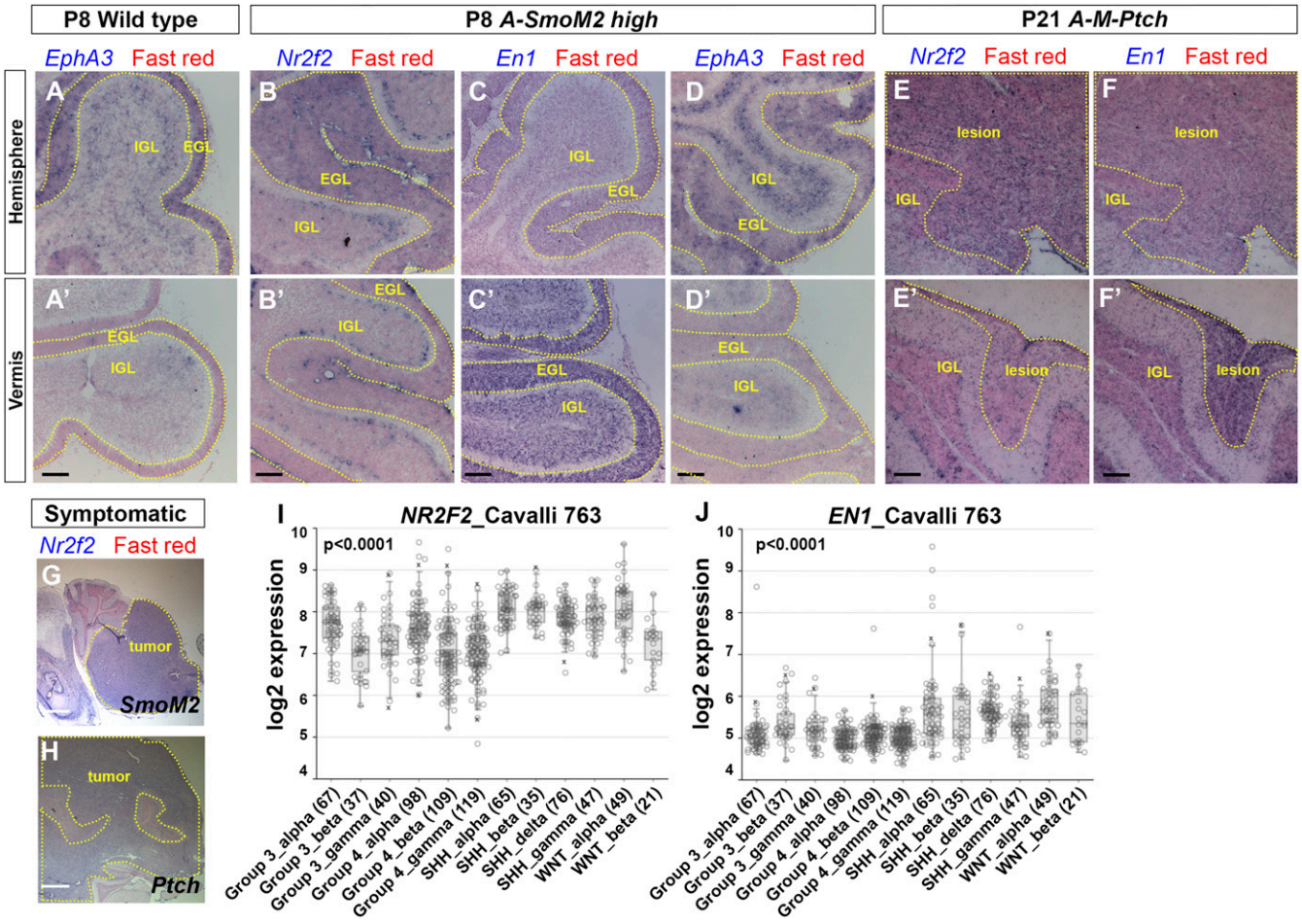

Fig. S9. Location-specific expression of *Nr2f2* and *En1* are maintained in cells with elevated SHH signaling. (*A*) RNA in situ hybridization of *EphA3* on sagittal sections in the H and V (*A′*) of P8 WT mice. (*B–D*) RNA in situ hybridization of *Nr2f2* (*B*), *En1* (*C*), and *EphA3* (*D*) on sagittal sections in the H and V (*B′–D′*) of P8 *A-SmoM2* administrated with a high dose of Tm at P2 (*A-SmoM2* high). (*E* and *F*) RNA in situ hybridization of *Nr2f2* (*E*) and *En1* (*F*) on sagittal sections in the H and V (*E′* and *F′*) of P21 *A-M-Ptch*. (Scale bars, 100 μm.) (*G–H*) RNA in situ hybridization of *Nr2f2* on symptomatic *A-SmoM2* (*G*) and *A-M-Ptch1* (*H*) mice. IGL, EGL, lesion, and tumor are marked by yellow dotted lines. (Scale bar, 1 mm.) (*I* and *J*) Expression of *NR2F2* (*I*) and *EN1* (*J*) in four subgroups of human MB samples using a second cohort to that shown in Fig. 5. Data were acquired from the R2: Genomics Analysis and Visualization Platform (https://hgserver1.amc.nl/cgi-bin/r2/main.cgi) and significance is calculated with a one-way ANOVA between groups.

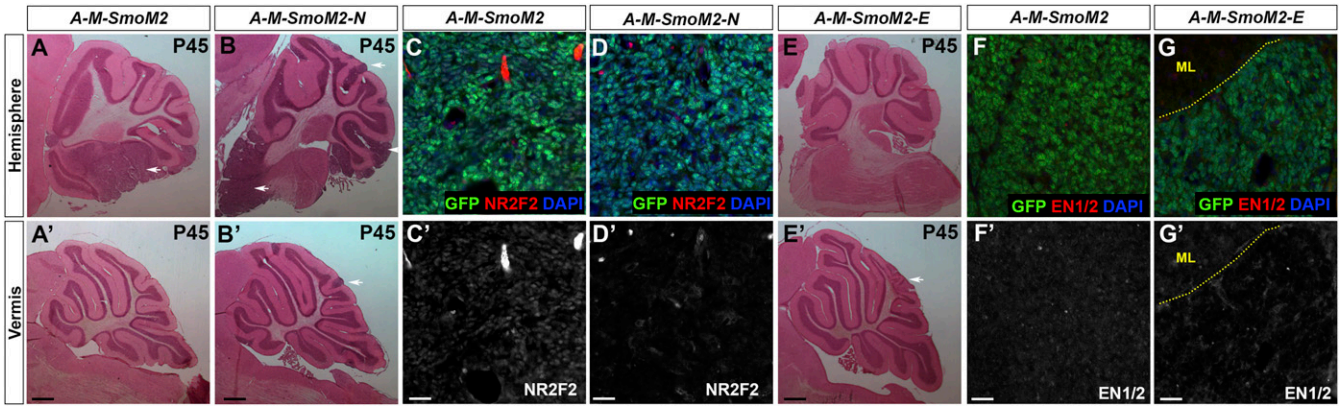

Fig. S10. Knocking out the location-specific genes does not affect *SmoM2* tumor progression. (*A* and *B*) H&E staining of sagittal sections in the hemisphere and vermis (*A′* and *B′*) of P45 *A-M-SmoM2* (*A*) and *A-M-SmoM2-N* (*B*) mice. (*C* and *D*) FIHC detection of GFP, NR2F2 (*C′* and *D′*) and on sagittal sections of P45 *A-M-SmoM2* (*C*) and *A-M-SmoM2-N* (*D*) mice. (*E*) H&E staining of sagittal sections in the H and V (*E′*) of a P45 *A-M-SmoM2-E* mouse. (*F* and *G*) FIHC detection of GFP, EN1/2 (*F′* and *G′*) and DAPI on sagittal sections of P45 *A-M-SmoM2* (*F*) and *A-M-SmoM2-E* (*G*) mice. White arrows in *A*, *B*, and *E* indicate lesions. [Scale bars, 500 μm (black) and 50 μm (white).]

Table S1. Mutation data and clinical characteristic of the 38 SHH-MB samples

Mutation	Age	Gender	Location	Histology
SMO	3	1	1	3
SMO	20	1	0	3
SMO	27	1	0	2
SMO	35	1	0	1
SMO	39	0	0	1
PTCH1	1	0	0	3
PTCH1	1	1	0	3
PTCH1	2	1	1	3
PTCH1	2	0	1	3
PTCH1	3	0	0	3
PTCH1	3	0	0	3
PTCH1	3	0	0	3
PTCH1	5	0	1	3
PTCH1	16	1	1	1
PTCH1	22	0	0	3
PTCH1	22	1	1	1
PTCH1	23	0	0	3
PTCH1	23	1	0	1
PTCH1	25	1	0	3
PTCH1	29	1	0	1
PTCH1	32	0	1	3
PTCH1	42	0	1	1
TP53 mut	10	0	0	2
TP53 mut	12	0	0	2
TP53 mut	13	1	1	2
TP53 mut	12	1	0	2
TP53 mut/*SUFU*	10	1	0	2
TP53 mut	7	1	1	2
TP53 mut	9	0	1	1
TP53 mut	10	1	0	1
TP53 mut	12	0	1	1
TP53 mut	12	0	0	2
TP53 mut	13	1	1	3
TP53 mut	14	0	0	2
TP53 mut	17	1	1	2
TP53 mut	21	0	0	2
SUFU	2	1	1	3
SUFU	3	0	1	1

Gender: 1, male; 0, female. Location: 1, vermis and IV ventricle; 0, cerebellar hemisphere. Histology: 1, classic, 2, large cell/anaplastic; 3, nodular-desmoplastic MB.

Table S2. Statistical results

Figures	Mean ± SEM and *P* value	Degree of freedom and *t*-value
Fig. 1*N*	H: 2.822 ± 1.006 mm^2; V: 0.078 ± 0.032 mm^2, $P = 0.0300$	$t(7) = 2.714$
Fig. 1*O*	H: 8.196 ± 2.295 mm^2; V: 1.461 ± 0.6897 mm^2, $P = 0.0175$	$t(4) = 3.903$
Fig. 3*A*	*A-M*: H 61.56 ± 3.49%; V 55.88 ± 0.92%, $P = 0.1757$	*A-M*: $t(3) = 1.765$
	A-M-SmoM2: H 94.39 ± 0.39%; V 89.90 ± 0.56%, $P = 0.0014$	*A-M-SmoM2*: $t(2) = 26.9$
	A-M-Ptch: H 87.40 ± 1.27%; V 79.19 ± 0.63%, $P = 0.0061$	*A-M-Ptch*: $t(2) = 12.71$
Fig. 3*B*	*A-M*: H 45.78 ± 0.39%; V 46.44 ± 1.08%, $P = 0.5534$	*A-M*: $t(3) = 0.6653$
	A-M-SmoM2: H 56.57 ± 1.64%; V 53.11 ± 1.18%, $P = 0.0876$	*A-M-SmoM2*: $t(2) = 3.153$
	A-M-Ptch: H 53.47 ± 0.77%; V 54.95 ± 0.89%, $P = 0.2602$	*A-M-Ptch*: $t(2) = 1.555$
Fig. 3*G*	*A-M-SmoM2*: H 32.69 ± 1.89%; V 36.07 ± 2.57%	
	A-M-Ptch: H 52.17 ± 6.32%; V 54.17 ± 4.96%	Two-way ANOVA
	Two-way ANOVA	Genotype: $F_{(1, 32)} = 18.9$
	Genotype: $P = 0.0001$; location: $P = 0.5382$	Location: $F_{(1, 32)} = 0.3871$
	Sidak post hoc test:	
	A-M-SmoM2 vs. *A-M-Ptch*	
	Hemisphere: $P = 0.0064$	
	Vermis: $P = 0.0114$	
Fig. 6*A*	*A-M-SmoM2-N*: H 87.13 ± 1.27%; V 89.7 ± 0.69%	
	A-M-SmoM2-N het: H 91.13 ± 0.24%; V 90.35 ± 0.34%	Two-way ANOVA
	Two-way ANOVA	Genotype: $F_{(2, 18)} = 14.58$
	Genotype: $P = 0.0002$; location: $P = 0.1196$	Location: $F_{(1, 18)} = 2.671$
	Sidak post hoc test	
	A-M-SmoM2 vs. *A-M-SmoM2-N*	
	Hemisphere: $P < 0.0001$	
	Vermis: $P = 0.9790$	
	A-M-SmoM2 vs. *A-M-SmoM2-N* het	
	Hemisphere: $P = 0.0088$	
	Vermis: $P = 0.8891$	
	A-M-SmoM2-N vs. *A-M-SmoM2-N* het	
	Hemisphere: $P = 0.0007$	
	Vermis: $P = 0.7505$	
Fig. 6*B*	*A-M-SmoM2-E*: H 92.72 ± 0.48%; V 90.35 ± 0.34%	
	Two-way ANOVA	Two-way ANOVA
	Genotype: $P = 6804$; location: $P = 0.0009$	Genotype: $F_{(1, 8)} = 0.1826$
	Sidak post hoc test	Location: $F_{(1, 8)} = 26.74$
	A-M-SmoM2 vs. *A-M-SmoM2-E*	
	Hemisphere: $P = 0.0916$	
	Vermis: $P = 0.0364$	
Fig. 6*C*	*A-M-SmoM2:* 1.37 ± 0.66 mm^2	
	A-M-SmoM2-N: 2.30 ± 0.97 mm^2	One-way ANOVA
	A-M-SmoM2-N het: 1.85 ± 0.72 mm^2	$F_{(2, 23)} = 0.3237$
	One way ANOVA $P = 0.7258$	
	A-M-SmoM2 vs. *A-M-SmoM2-N*: $P = 0.7029$	
	A-M-SmoM2 vs. *A-M-SmoM2-N* het: $P = 0.9044$	
	A-M-SmoM2-N vs. *A-M-SmoM2-N* het: $P = 0.9153$	